ous pump infusion of somatostatin analogue SMS 201-995 versus subcutaneous injection schedule in acromegalic patients. *Clin Endocrinol* 1987, 27, 297–306.
26. Armstrong DG, Duclos MJ, Goddard C. Biological activity of insulin-like growth factor purified from chicken serum. *Domest Anim Endocrinol* 1990, 7, 383–393.
27. Tanaka T, Shiu RPC, Gout PW, *et al.* A new sensitive and specific bioassay for lactogenic hormones: Measurement of prolactin and growth hormone in human serum. *J Clin Endocrinol Metab* 1980, 51, 1058–1063.
28. Anderson E, Morten H, Wang DY, Burns P, Birch J, Howell A. Serum bioactive lactogenic hormone levels in women with familial breast cancer and their relatives. *Eur J Cancer Clin Oncol* 1989, 25, 1719–1725.
29. Malarkey WB, Schroeder LL, Stevens VC, James AG, Lanese RR. Disordered nocturnal prolactin regulation in women with breast cancer. *Cancer Res* 1977, 37, 4650–4654.
30. Bartsch C, Bartsch H, Fuchs U, Lippert TH, Bellmann O, Gupta D. Stage-dependent depression of melatonin in patients with primary breast cancer. Correlation with prolactin, thyroid-stimulating hormone and steroid receptors. *Cancer* 1989, 64, 426–433.
31. Thorner MO, Rogol AD. Neuroendocrine regulation of growth hormone secretion. In Underwood LE, ed. *Human Growth Hormone: Progress and Challenges*. New York, Marcel Dekker, 1988, 113–130.
32. Love RR, Rose DP. Elevated bioactive prolactin in women at risk for familial breast cancer. *Eur J Cancer Clin Oncol* 1985, 21, 1553–1554.
33. Lamberts SWJ, Oosterom R, Neufeld M, del Pozo E. The somatostatin analog SMS 201-995 induces long acting inhibition of growth hormone secretion without rebound hypersection in acromegalic patients. *J Clin Endocrinol Metab* 1985, 60, 1161–1165.
34. Setyono-Han B, Henkelman MS, Foekens JA, Klijn JGM. Direct inhibitory effects of somatostatin (analogues) in the growth of human breast cancer cells. *Cancer Res* 1987, 47, 1566–1570.
35. Fekete M, Wittliff JL, Schally AV. Characteristics and distribution of receptors for (D-TRP6)-luteinising hormone-releasing hormone, somatostatin epidermal growth factor and sex steroids in 500 biopsy samples of human breast cancer. *J Clin Lab Anal* 1989, 3, 137–147.

Acknowledgements—We are most grateful to Sandoz Pharmaceuticals for supplying the bromocriptine and Sandostatin® used in this study. We wish to thank Dr C. Goddard (AFRC, Roslin) for his generous gift of IGF-I antiserum. We thank Dr E. Pearson and Mrs J. Miller for their help with the sequential venous sampling. This study was supported by the Endowment Fund of the Christie Hospital.

Eur J Cancer, Vol. 29A, No. 2, pp. 217–225, 1993.
Printed in Great Britain

0964–1947/93 $5.00 + 0.00

Preferential Antibody Targeting to Small Lymphoma Metastases in the Absence of the Primary Tumour

Udo Schmid, Volker Schirrmacher, Frank Momburg and Siegfried Matzku

Targeting of spontaneous liver metastases of the ESb.MP murine lymphoma was achieved with anti-CD2 monoclonal antibody (MAb) 12-15A, which does not react with normal liver tissue. Using quantitative autoradiography on whole body sections of animals that had received a standard dose of 1.1 MBq of ^{125}I-labelled monoclonal antibody, metastases accumulated up to > 90% of the injected dose per gram (id/g). The average uptake of primary tumour lesions was at a low level of 24 Bq/mg (corresponding to 2.2% id/g) because of highly non-uniform accumulation, while metastatic lesions were all above 50 Bq/mg. Uptake was particularly pronounced in animals tested after resection of the primary tumour: 85% of metastases showed levels above 300 Bq/mg, which was the upper limit of uptake in metastases of non-resected animals. These findings demonstrate the potential of the antibody approach with regard to attacking residual metastatic lesions after debulking.
Eur J Cancer, Vol. 29A, No. 2, pp. 217–225, 1993.

INTRODUCTION

THERE IS increasing evidence to show that monoclonal antibodies (MAb) are non-uniformly accumulated in varying tumour types [1–7], the pattern being dependent on tumour architecture and the nature of the target antigen. We set out to analyse whether small metastatic foci would show a more uniform accumulation, thereby reaching high uptake levels as observed in some segments of macroscopic tumour nodules, or whether they are secluded by inherent accessibility barrier(s). The ESb.MP murine lymphoma model [8] was chosen to address the question. ESb.MP metastasises reproducibly into the liver irrespective of the mode of implantation (i.e. intradermal or subcutaneous) and of surgical removal of the primary inoculum. Targeting of primary and secondary processes was successfully achieved with MAb 12-15A, while non-specific antibodies or fragments showed no marked accumulation [9]. MAb 12-15A [10] recognises an epitope of murine CD2 differentiation antigen and possibly also of the Fc receptor [11, 12], the antigen density being much higher on ESb.MP lymphoma cells than on murine lymphocytes [10]. Accumulation of labelled MAb 12-15A could be selectively directed towards lymphoma tissue by pretreatment of animals with the unlabelled MAb, the effect

Correspondence to S. Matzku.
S. Matzku is at the Department of Medicinal Chemistry, E. Merck, Pf. 4119, D-6100 Darmstadt 1; U. Schmid is at the Institut für Radiologie und Pathophysiologie; and F. Momburg and V. Schirrmacher are at the Institut für Immunologie und Genetik, Krebsforschungszentrum, Im Neuenheimer Feld 280, D-6900 Heidelberg, F.R.G.
Revised 14 July 1992; accepted 6 Aug. 1992.

being most likely due to differential modulation of the target antigen in normal lymphatic vs. lymphoma tissue [9]. The biodistribution of ^{125}I-labelled 12-15A was such that very low levels of radioiodine were observed in the liver, thus allowing for the detection of small and/or weakly accumulating lesions in this organ.

With respect to detection and quantification of accumulation of radioiodinated MAb in small lesions, quantitative autoradiography methodology is unique in combining high spatial resolution with quantitative evaluation of the signal [13–15]. In the present context it was necessary to establish and validate additional procedures for identifying the outline of accumulating areas in autoradiograms and for the assessment of radioactivity concentrations in small sources. The methodology has been described in detail in a preceding publication [16]. As a further means of verifying the nature and the size of hot spots in autoradiographs, immunohistological staining of metastatic foci was performed in neighbouring sections. Thus, we implemented the prerequisites for a quantification of MAb uptake in small spontaneous metastases, which was not feasible with previously used methodology.

MATERIALS AND METHODS

Tumour transplants

ESb.MP cells were injected intradermally into the flank of DBA/2 mice (2×10^5 tissue cultured cells per animal). In most experiments the local tumour was excised 3 weeks after inoculation and a variable number of liver metastases ranging from 0.1 to 5 mm in diameter were detected in almost every animal after a further 10 days. When MAb injection was started, animals still had a life expectancy of roughly 7 days. In one experiment, subcutaneously implanted tumours were left in place and MAb was injected 4 weeks after inoculation of tumour cells.

Monoclonal antibodies

MAb 12-15A (rat IgG1; [10]) was purified by chromatography on protein A and Mono Q columns (Pharmacia). The MAb was labelled with ^{125}I by the use of IODOGen [17], specific activities being adjusted to 200–300 kBq/μg protein. As a control antibody with irrelevant specificity we used F(ab')$_2$ fragments derived from HOPC 1 (murine IgG2a), the rationale for using fragments rather than intact IgG being a short half life *in vivo* comparable with intact 12-15A [9].

Administration of labelled MAb

Tumour-bearing mice were given iodide in the drinking water the day before application of labelled MAb. Animals were pretreated with unlabelled antibody 12-15A [F(ab')$_2$ fragments, 20 μg per animal intravenously], 2 h before application of the labelled MAb. A standard dose of 1.1 MBq of ^{125}I-labelled specific and control MAb was used throughout.

Quantitative autoradiography

The procedure has been described in detail in a previous paper [16]. 48 h after intravenous injection of labelled MAb, animals were sacrificed by extensive ether anaesthesia and frozen in isopentane/dry ice. Alternatively, livers were first dissected and then subjected to freezing. Samples were embedded in precooled methylcellulose (2.5% w/v). Frozen blocks were cut with a Reichert–Jung whole body cryotome (Nussloch, FRG), 20 μm sections being collected on adhesive tape. These were lyophilised and placed on X-ray film (Kodak X-OMAT AR), which was exposed for 2–4 weeks. Film density was analysed using a scanning densitometer (Joyce Loebl) and transformed into a digital greylevel matrix. Transformation into a dose matrix was then performed using a calibration curve which was established by exposing tissue paste standards containing graded doses of ^{125}I-labelled protein [16, 18] under identical conditions. (N.B. Digital matrices obtained by transformation of greylevel matrices using a density-to-radioactivity calibration curve are nevertheless called dose matrices, because the X-ray film detects radiation rather than radioactivity.) In the digital dose matrices, hot spots representing metastases were analysed by program elements that supported the region-of-interest procedure, or the calculation of dose profiles through individual hot spots, or the establishment of isodose lines. Areas of hot spots in a given liver section were determined by identification of the dose level in the flanking region (steepest slope) of two dose profiles through the spot and by drawing an isodose line at the thus defined level [16]. The amount of radioactivity (in terms of Bq per unit volume) contained within this area was determined by integration within an isodose-line set at 1% above background level. Both elements of analysis are illustrated in Fig. 1, using the example of a small standard source of known geometry and known radioactivity content.

Immunohistology

Cryostat sections (5 μm thick) from metastasis-containing livers were stained with MAb 12-15A in a first step, and with peroxidase-labelled goat anti-rat Ig in a second step, following standard procedures. Neighbouring sections (5 μm thick) were mounted on cover slips and were placed on X-ray films as described above, exposure times being prolonged by a factor of two to compensate for the smaller section thickness as compared with whole body sections.

RESULTS

Biodistribution of specific and control MAb in mice with ESb.MP transplants

The typical appearance of an animal with an ESb.MP transplant and spontaneous liver metastases 48 h after inoculation of ^{125}I-labelled 12-15A is shown in Fig. 2a, b. High MAb accumulation was found in both types of tumour tissue. In addition, residual radioactivity was localised in lymph nodes and spleen as well as in unidentified small foci in the skin and in oro-nasal mucosae. The specificity control could not consist of simply injecting intact irrelevant antibody because this would not allow for the influence of normal lymphoid tissue on biodistribution and pharmacokinetics. Therefore, we used F(ab')$_2$ fragments of irrelevant MAb HOPC 1 since these mimicked the general pharmacodynamics of intact 12-15A fairly closely. The control preparation visualised areas of high blood content and/or high perfusion, e.g. large hepatic vessels, and some but not all hepatic metastases (Fig. 2c, d). Furthermore, radioactivity persisted for some time in haemorrhagic areas, but disappeared completely after 48 h p.i. (not shown), while specific retention of MAb 12-15A in lymphoma tissue was still impressive at time points $\geq$ 48 h.

The nature of hot spots of radioactivity accumulation in the liver was verified by immunohistology. What was positively stained in the autoradiographs and showed a high signal in digital matrices, corresponded exactly to the peroxidase-stained areas of metastatic lesions in adjacent sections (Fig. 3). Hence, *in vivo* targeted MAb—in the case of autoradiography—and *in vitro* applied MAb—in the case of immunohistology—were found to stain the same processes, thus proving that hot spots in

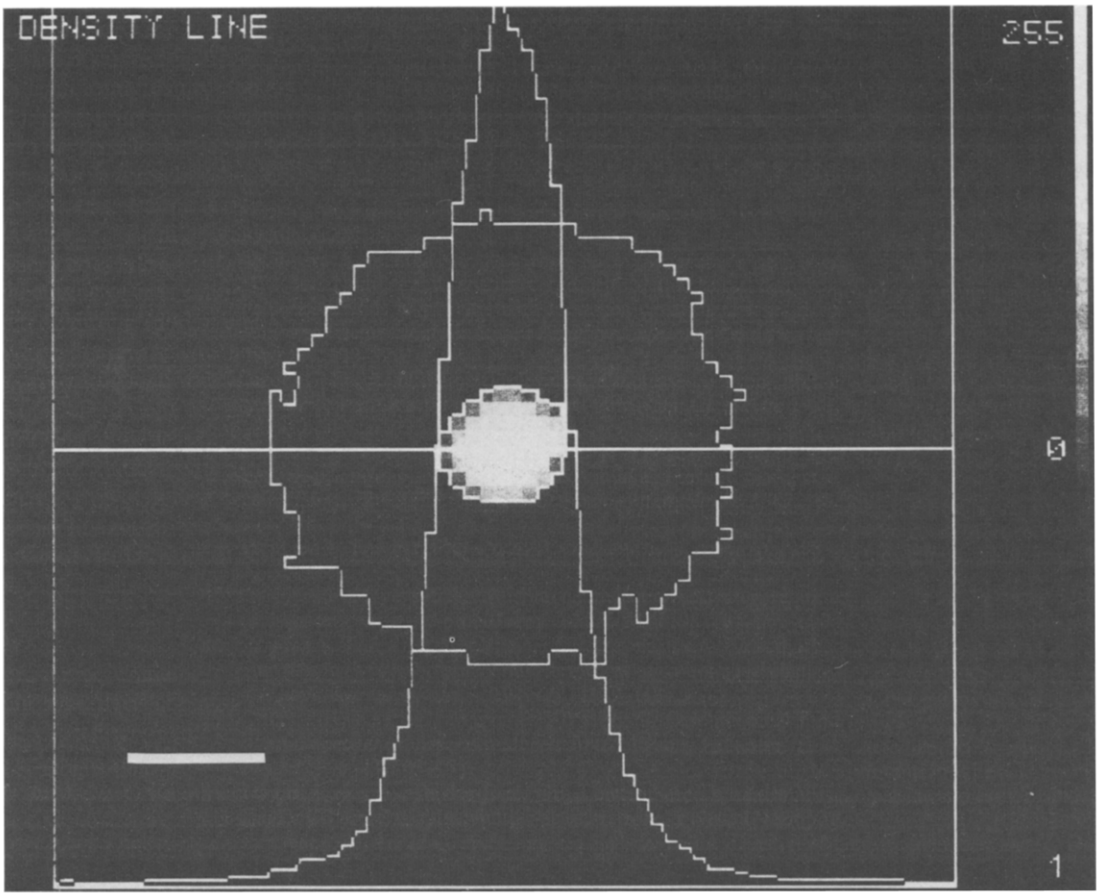

Fig. 1. Schematic presentation of the method used for evaluating the areas and the radioactivity content of small radioactive sources. A cylindrical phantom with a diameter of 400–450 μm filled with ^{125}I-labelled tissue paste was sectioned and subjected to quantitative autoradiography. The dose matrix of the section is shown, together with one of two dose profiles through the centre of the spot. These were used for defining the contours of the source according to the steepest slope criteria and the area of dose integration according to the 1% above background criteria. The grey scale of the matrix was chosen in a way to highlight dose elements within the source, while dose elements in the halo region can only be judged from the steps of the dose profile. Length of the bar = 0.5 mm.

autoradiographs of liver samples were indeed derived from lymphoma metastases. Moreover, immunohistology confirmed that small liver lesions were homogeneously packed with non-necrotic lymphoma cells, as it was suggested by homogeneously stained spots in the autoradiographs.

Quantification of MAb uptake in defined areas

The question was asked how uptake levels in liver metastases would compare with those of the local tumour. The methodological prerequisite was a procedure of transforming film densities produced by small radioactive sources into dose distribution and calculating radioactivity concentrations on the basis of predefined assumptions as to dose distribution in and around the actual radioactive sources (see Fig. 1 and [16]). Fig. 4 shows both the greylevel matrix of a liver segment with many metastases of different sizes and the dose matrix derived therefrom. Fig. 4a and b differ with respect to magnification and scale. Visual inspection of accumulation patterns was greatly facilitated by the colour scale on the screen, which is only poorly reflected by the black and white photograph, but especially by the clearly discernible steps of dose profiles (see Fig. 1).

The diagram in Fig. 5a gives an overview of the size distribution of hot spots as observed in the liver of animals after resection of the primary lesion (n = 15 animals). Data were collected from six sections per liver at a 0.5 mm distance, thus hopefully addressing the majority of lesions in individual livers. The smallest lesions to be detected and evaluated had diameters between 0.1 and 0.2 mm, although dense spots with smaller diameters were occasionally observed. On the other hand, lesions with diameters > 1 mm comprised less than 10% of hot spots analysed.

A further question was how relative uptake in metastases correlated with the apparent diameter. It was not possible to get an exact answer because it could not be judged from the autoradiograms whether an individual hot spot reflected a section through, e.g. the centre of a small metastasis or through the pole of a large metastasis. Despite this limitation, a trend towards an increase of uptake with increasing size became apparent in seven of 11 animals analysed; Fig. 5b giving a representative example. Taking together the information from all sections analysed, an increase was noted from 400 Bq/mg in the smallest detectable hot spots to > 700 Bq/mg (corresponding to > 64% injected dose per g) in spots with diameters greater than 0.8 mm.

Comparison of 12-15A uptake in the primary lymphoma and in liver metastases

Since MAb 12-15A uptake in spontaneous liver metastases was greatly influenced by the presence of primary tumour

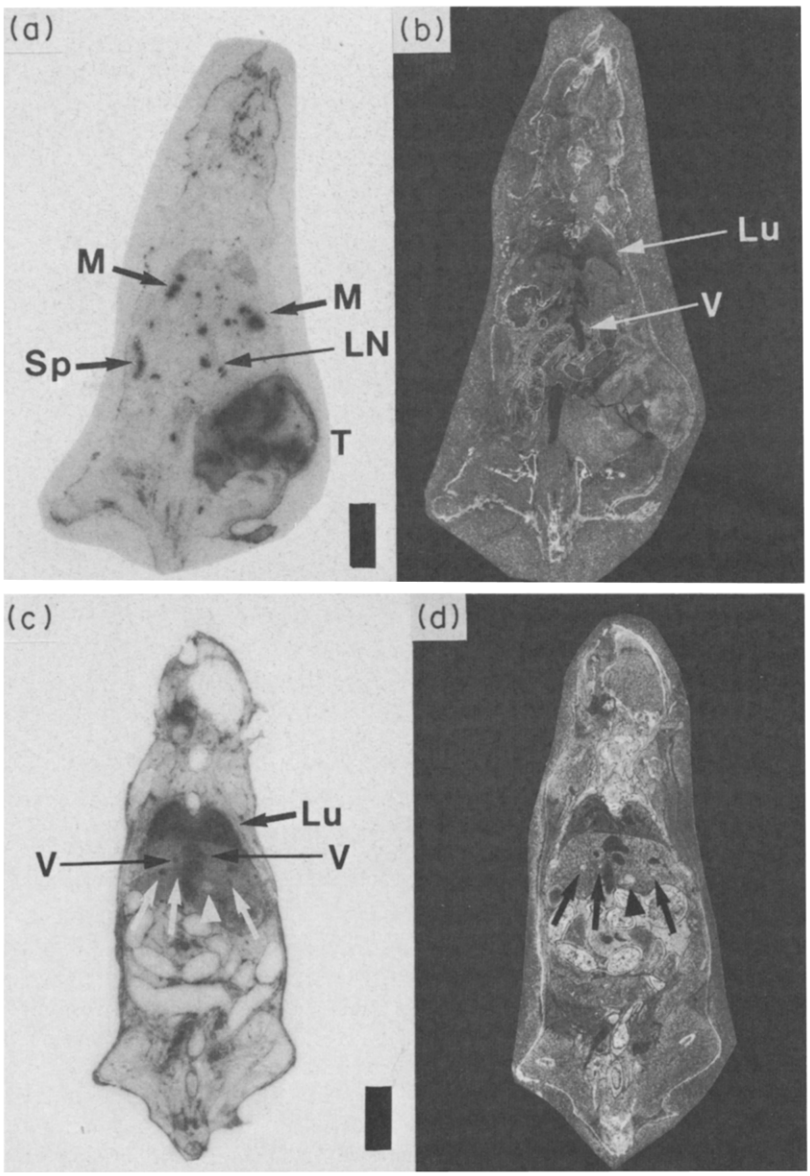

Fig. 2. Whole body sections and autoradiographs from mice after application of [^{125}I]12-15A or non-specific control antibody [F(ab')$_2$ fragment]. Autoradiogram (a) and section (b) from a mouse with local tumour in the lower right flank (T) and liver metastases (M) 48 h after application of [^{125}I]12-15A (IgG). Pretreatment with unlabelled 12-15A [20 μg F(ab')$_2$, at −2 h]. V, Blood vessel; Lu, lung; Sp, spleen; LN, lymph node. Note the almost complete clearance of radioactivity from the blood as well as the highly non-uniform radioactivity uptake in the local tumour. Autoradiograph (c) and section (d) of a mouse with liver metastases 12 h after application of ^{125}I-labelled control MAb [HOPC 1, F(ab')$_2$]. Symbols as in (a, b). Note simultaneous presence of highly perfused [white arrows in (c), black arrows in (d)] and weakly perfused lesions (white and black arrowheads) in the same liver specimen. Length of bars = 1 cm.

masses, autoradiographic evaluation of radioactivity accumulation was performed in animals that had or had not undergone resection of the subcutaneous lymphoma (Fig. 5c). When integrating over the whole cross-section of the primary tumour (n=9 animals), the average uptake level was at 24 Bq/mg tissue. Intratumoral hot spots showed uptake levels in the range of 50–700 Bq/mg (average level in hot spots 235 Bq/mg). In the same animals, liver metastases showed an uptake in the range of 50–300 Bq/mg (average 135 Bq/mg), the difference to levels in intratumoral hot spots not being significant. In the absence of the primary lymphoma, i.e. in animals tested 10 days after resection, MAb accumulation in liver metastases was markedly higher: 85% of lesions showed levels above 300 Bq/mg, which was the upper limit of accumulation in metastases of non-resected animals.

Uniformity vs. non-uniformity of MAb uptake in metastases of different size

Liver foci with diameters in the range of 0.1–0.8 mm were composed of homogeneously staining lymphoma cells. This was the result of a comparison of immunohistology and autoradiography on neighbouring sections (see Fig. 3). With respect to larger size lesions, autoradiographic images were correlated to the visual aspect of lyophilised (unstained) tissue sections, metastases being bona fide identified by their pale aspect as opposed to the light-brown colour of liver parenchyma. In Fig. 6a, c

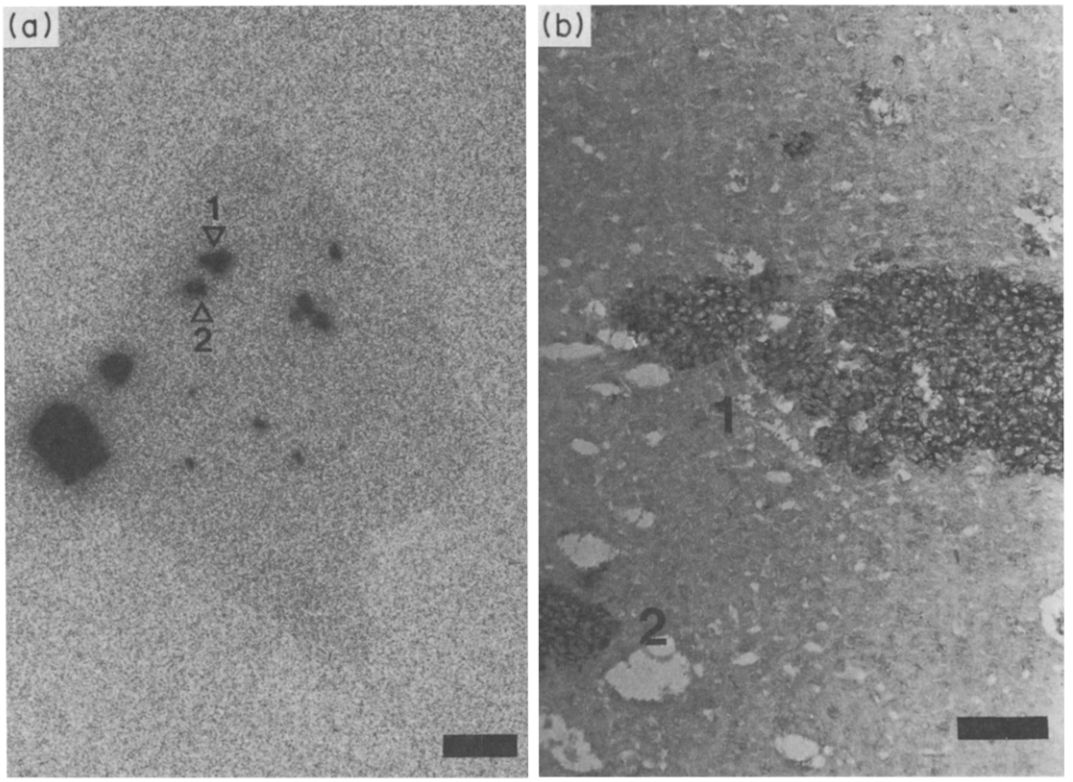

Fig. 3. Comparison of immunohistological and autoradiographic visualisation of liver metastases in adjacent sections. (a) Autoradiography after injection of ^{125}I-labelled 12-15A (bar = 1 mm). The lesions 1 and 2 (open arrowheads) are partially depicted in (b). (b) Immunohistology of metastases on adjacent sections (bar = 50 μm). The lesions stained with the 12-15A and peroxidase-labelled goat anti-rat Ig *in vitro* correspond exactly with respect to size and diameter to their autoradiographic image as obtained after treatment with [^{125}I]12-15A *in vivo*.

two liver samples are shown which differ with respect to the metastatic load, thus depicting a collection of characteristic accumulation patterns (identified by numbers 1 to 6). We categorised small, intermediate and large size metastases with uniformly dense staining, large metastases with uniformly weak staining, and large metastases with different patterns of non-uniform staining. Large metastases with uniformly high uptake were infrequent, their occurrence being restricted to animals with few lesions (Fig. 6a, b), thus indirectly corroborating the finding that uptake levels were lowered by a large tumour burden. The majority of large metastases were encircled by a macroscopically visible blood vessel and/or a haemorrhagic zone (Fig. 6c). In the autoradiographic images, pronounced staining was found in the vicinity of such peripheral blood structures, while equally large lesions that were devoid of a peripheral blood pool showed moderate to low accumulation of the radioactive MAb (Fig. 6d).

DISCUSSION

The targeting of ESb.MP lymphoma lesions with MAb 12-15A is complicated by the fact that the antigen is also found on the surface of normal lymphocytes [9, 11, 12]. Competitive binding by normal lymphatic tissue can be suppressed by dose escalation, presumably because of a modulatory removal of the antigen from normal lymphocytes as opposed to a more stable MAb binding to ESb.MP cells. With the pre-injection regime used in this study we achieved operational selectivity of lymphoma tissue targeting. Similar experiences were also obtained in another lymphoma model system [19].

The central problem of this study was quantification of radioactivity accumulation in small volume elements as visualised by autoradiography. Due to the finite range of ^{125}I (electromagnetic) radiation, the true outlines of a source are not directly visible in the autoradiographs and the area to be chosen for dose integration is not defined *a priori*. The measures taken to overcome the problem have been described and critically evaluated in the preceding paper [16]. Moreover, it was verified that hot spots in autoradiograms were in fact derived from liver metastases. This was achieved by subjecting neighbouring liver sections to autoradiography and immunohistology. Indeed, small metastatic foci were composed of uniformly staining lymphoma cells. In case of larger lesions (> 0.8 mm diameter) with non-uniform accumulation (see Fig. 6), which represented the exception rather than the rule, the determination of radioactivity concentrations was restricted to accumulating areas within individual metastasis but not to the metastatic lesion as such. In these cases, the "grid overlay" technique [13] would have been preferable, although this was not feasible due to the impossibility of staining whole body sections. A more important restriction resulted from the fact that in two-dimensional sections it could not be determined whether a small hot spot represented the pole of a large or the central portion of a small lesion. This problem will be solved as soon as sufficient computer capacity is available for compiling consecutive autoradiographs to yield three-dimensional radioactivity distribution data.

In view of these restrictions, it was not possible to exactly measure the size dependence of radioactivity accumulation in metastases. Yet, we observed a trend towards increased uptake with increasing lesional size up to diameters of about 1 mm. It is hypothesised that the accessibility of very small intrahepatic lesions is similar to that of normal liver tissue, while medium-sized lesions experience an additional benefit as soon as they are autonomously supplied by newly formed tumour vessels.

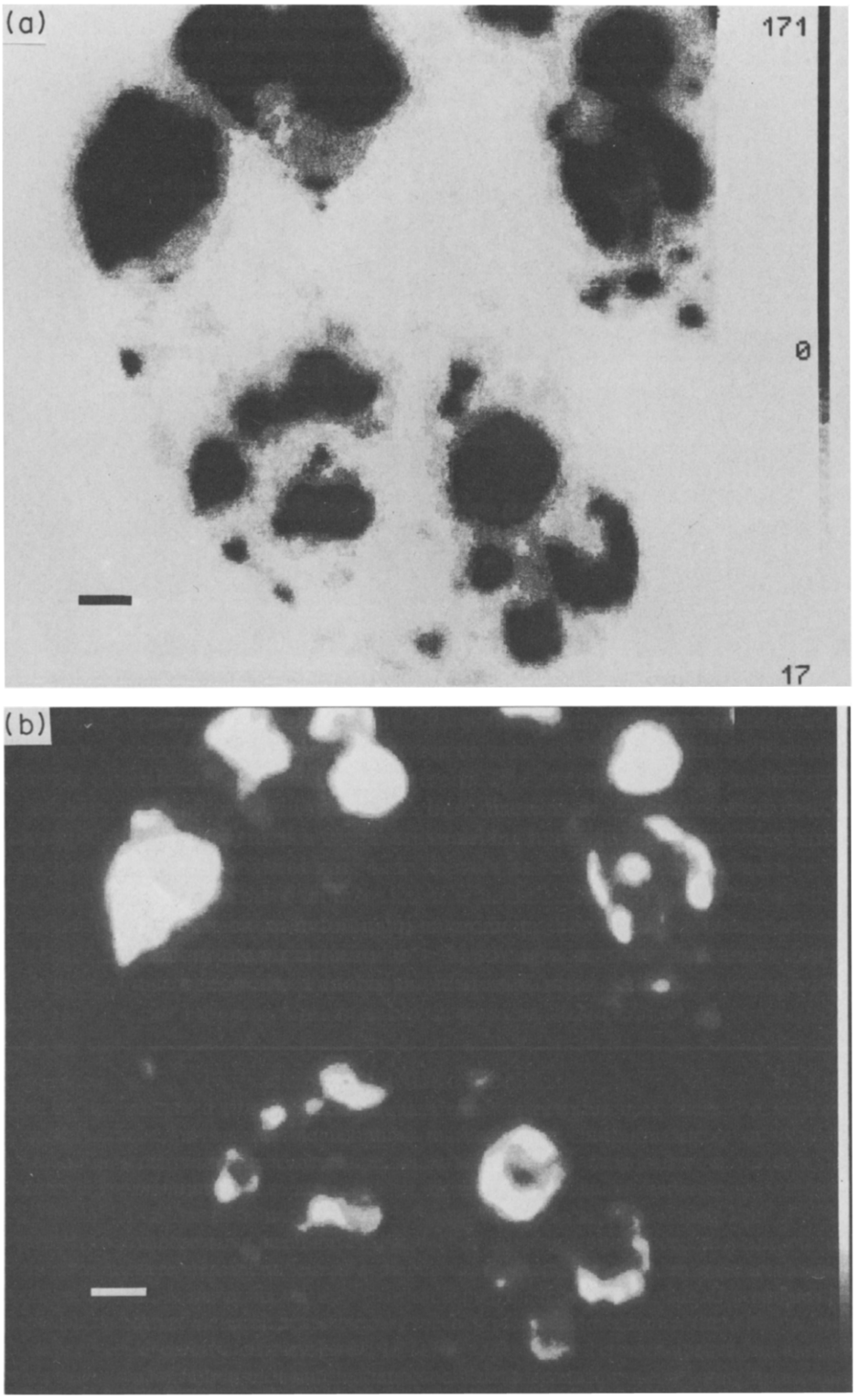

Fig. 4. Greylevel matrix and dose matrix of a liver with multiple metastases 48 h after application of [^{125}I]12-15A. (a) Greylevel matrix; (b) dose matrix. When working in the dose matrix screen, individual hot spots were zoomed in order to facilitate the drawing of the isodose lines which putatively represented the contours of accumulating areas, as well as the isodose lines which defined the areas used for integration of the total radioactivity content of the source. N.B. Due to different colour scales used in both matrices, background levels are represented by white areas in (a) and by black areas in (b). Length of bars = 1 mm.

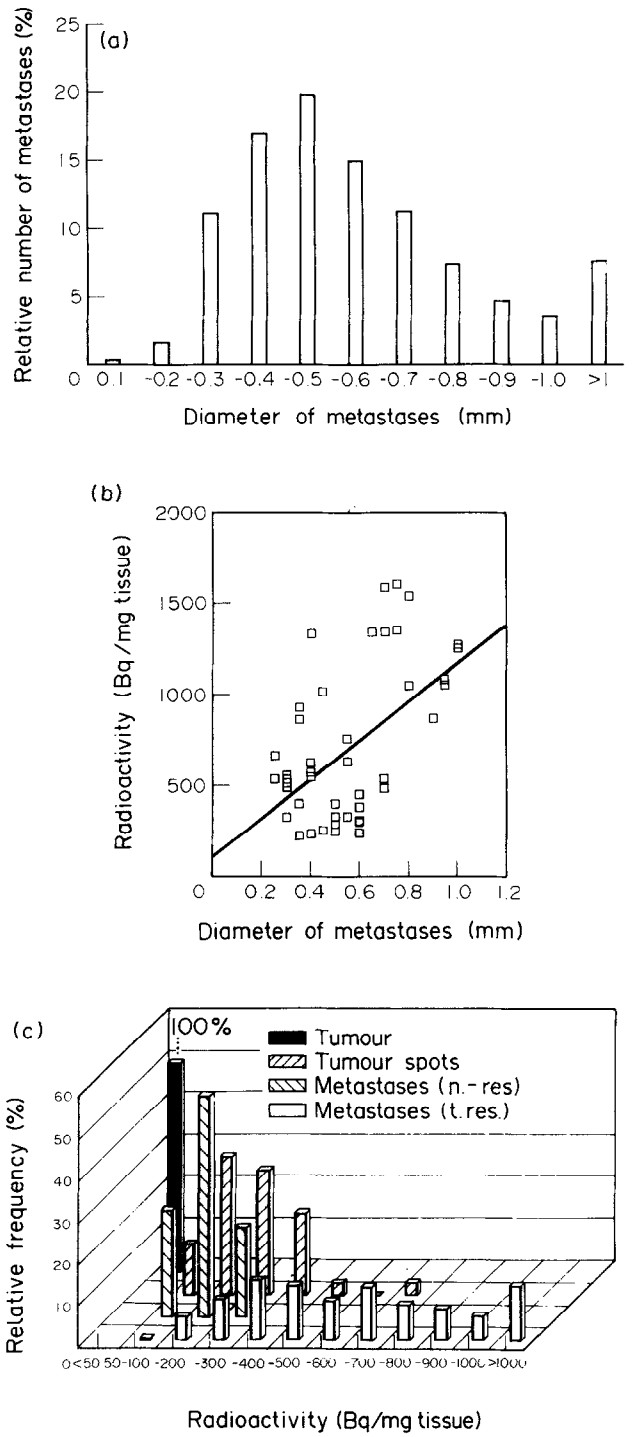

Fig. 5. Analysis of liver metastases with respect to size and radioactivity uptake. (a) Relative frequency of metastases sorted according to apparent diameter of lesions (n = 15, six sections per animal). (b) Size dependence of radioactivity uptake in one single liver sample. Two well separated sections with a total of 47 hot spots were analysed. Regression line, n = 0.53. (c) Radioactivity concentration per mg tissue in tumours and metastases of animals with and without resection of the primary tumour. The histogram indicates the average radioactivity concentration in the primary tumour and in intratumoral hot spots (n = 9, six sections per animal). Note that all primary tumours fall in the category < 50 Bq/mg (mean value 24 Bq/mg). Hence, the frequency is 100% as indicated above the column. Furthermore, uptake in metastases of animals bearing the primary tumour (n. -res.; n = 9) is compared with uptake in metastases of animals after resection of the primary tumour (t. res; n = 15). Since a total of 1.1 MBq of [^{125}I]12-15A was injected per animal, 100 Bq/mg correspond to 9.1% of the injected dose per g tissue.

Large tumour masses, especially the primary lymphoma, showed a markedly lower average uptake than small metastases because of high non-uniformity. Additionally, the absolute uptake in metastases of primary tumour-bearing animals was lower than in metastases of animals tested after resection, i.e. maximum values were 300 Bq/mg and > 1000 Bq/mg, respectively. This is reflecting the fact that the administered doses of labelled MAb were clearly in the sub-saturating range. With respect to the question of whether a 24 Bq/mg accumulation in the primary lymphoma could explain the marked reduction at the level of metastases, it has to be taken into account that the overall mass of metastatic tissue was generally low compared with the mass of the primary lymphoma. Furthermore, uptake levels recorded after 48 h may represent an underestimation of the integral uptake because of slow processing of iodinated MAb 12-15A in tumour tissue. Taking everything together, our results support the idea that small metastases are a preferential target for antibody, especially in the absence of primary tumour masses and/or at subsaturating antibody concentrations. This is good news with respect to the systemic application of therapeutical antibody in an adjuvant setting.

When metastases were greater than 1 mm, marked variability in patterns and levels of uptake was observed. Uptake was both high and uniform in animals with few metastases, again suggesting that relative uptake of 12-15A was increased with decreasing tumour burden. In animals with advanced metastatic growth, uptake in larger metastases was generally non-uniform or uniformly low. When inspecting large metastases, segments of high uptake were found almost invariably in the vicinity of prominent vascular structures, which often encircled the lesions (Fig. 6c). According to our evidence from haematoxylin and eosin-stained sections, these structures correspond to what has been described as 'giant capillaries' or 'lacunae' [20, 21], and also to haemorrhagic necrosis in the vicinity of leaky vessels. Due to the lack of regulation of blood flow in those vessels, their large diameters, and the irregular architecture of vessel walls, stasis and diapedesis of blood components may become the dominant feature. This may lead to a transient storage of antibodies [22] and to a slow release into tumour tissue, especially if the integrity of membranous tissue barriers is disturbed.

From our data it is concluded that metastases of an intermediate size of 0.4–1 mm are the best targets for monoclonal antibodies, the window in size being relatively narrow. It is obvious that the optimal size for accumulation (in the mouse) is far below the detection limit of scintigraphic devices. We are aware of one other report on MAb uptake in experimental metastases, which is based on a colon carcinoma model in the hamster, metastatic spread being directed to the lung [23]. High uptake in small lesions was observed in this system too, but no attempt was made to quantify and to compare metastatic lesions with the primary tumour. In view of clinical results pointing to a difference in immunolocalisation of lung metastases as opposed to, e.g. liver metastases or regional recurrences of colorectal tumours [24], it remains to be systematically elaborated to what extent preferential targeting of small lesions as opposed to large tumour masses is influenced by the biology of the target antigen, the architecture of metastatic tissue, the normal tissue hosting tumour growth, and—after all—by the species bearing the tumour.

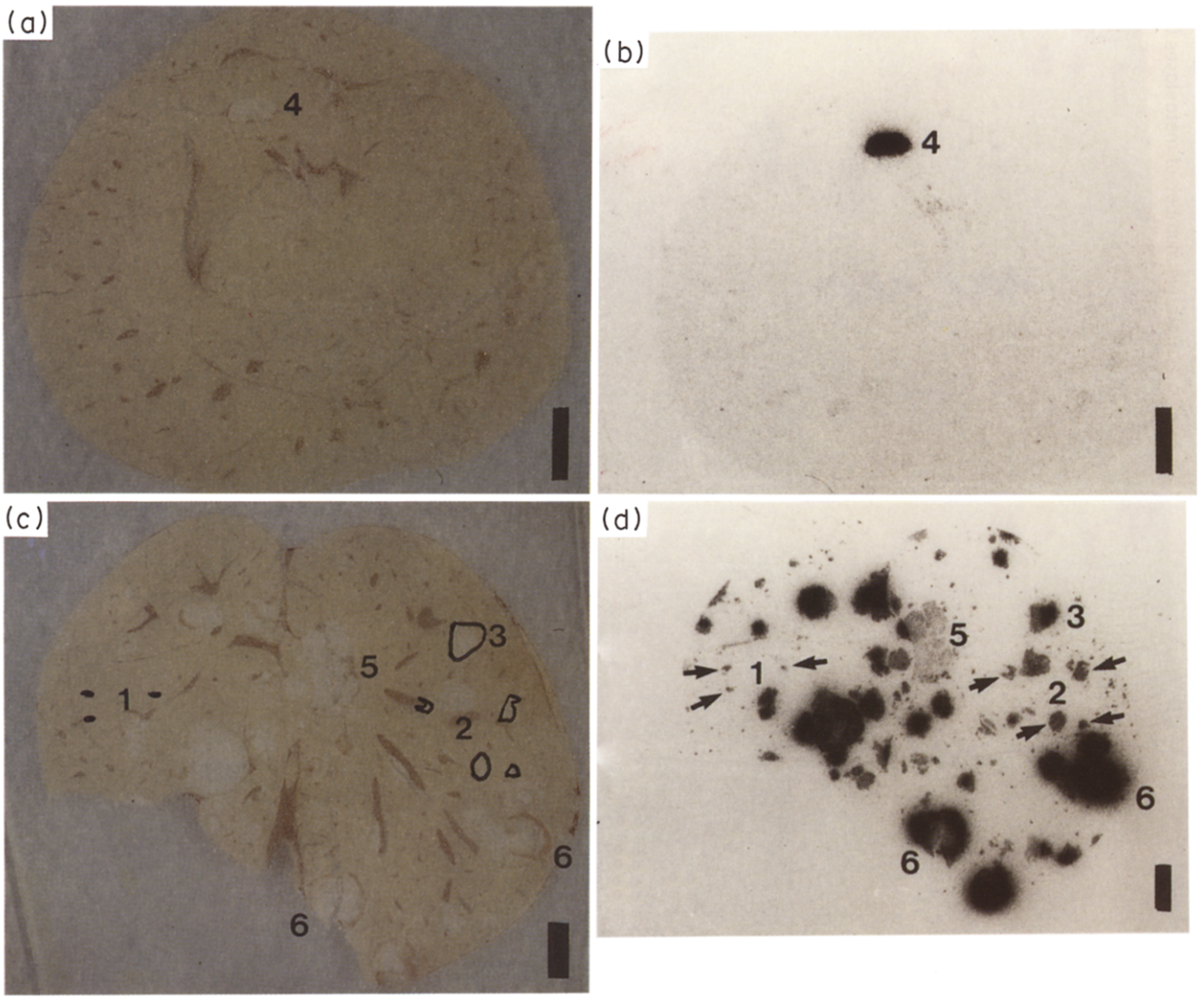

Fig. 6. Autoradiographic visualisation of metastases in individual liver samples. (a), (c) Lyophilised liver sections, unstained. (b), (d) Corresponding autoradiographs (X-ray films prior to any processing). Large vessels (dark brown structures) and large metastases (pale areas) are clearly visible in the sections, while faintly visible lesions are encircled by black lines. Clearance of radioactivity out of the blood was virtually complete as corresponding areas in the autoradiographs showed background density. Typical metastatic lesions and corresponding spots on X-ray images are identified by numbers which relate to the following categories: 1, 2, 4, small, intermediate size, large metastases with uniform uptake; 3, large size metastasis showing a gradient uptake; 5, large metastasis, low uptake; 6, large metastases, highly non-uniform uptake. Arrows are pointing to several representatives of the small (left-hand side of autoradiograph) and the intermediate size category (2; right-hand side).

1. Moshakis V, Ormerod MG, Westwood JH, Imrie S, Neville AM. The site of binding of anti-CEA antibodies to tumour CEA *in vivo*: an immunochemical and autoradiographic approach. *Br J Cancer* 1982, **46**, 18–21.
2. Cobb LM, Humphreys JA, Harrison A. The diffusion of a tumour-specific monoclonal antibody in lymphoma infiltrated spleen. *Br J Cancer* 1987, **55**, 53–55.
3. Matzku S, Tilgen W, Kalthoff H, Schmiegel WH, Bröcker EB. Dynamics of antibody transport and internalization. *Int J Cancer* 1988, **2** (Suppl.), 11–14.
4. Buchegger F, Haskell CM, Schreyer M, *et al.* Radiolabelled fragments of monoclonal antibodies against carcinoembryonic antigen for localization of human colon carcinoma grafted into nude mice. *J Exp Med* 1983, **158**, 413–427.
5. Sands H, Jones PL, Shah SS, Palme D, Vessella RL, Gallagher BM. Correlation of vascular permeability and blood flow with monoclonal antibody uptake by human Clouser and renal cell carcinoma xenografts. *Cancer Res* 1988, **48**, 188–193.
6. Pervez S, Epenetos AA, Mooi WJ, *et al.* Localization of monoclonal antibody AUA1 and its F(ab')2 fragments in human tumour xenografts: an autoradiographic and immunohistochemical study. *Int J Cancer* 1988, **3** (Suppl.), 23–29.
7. Chen F-M, Epstein AL, Li Z, Taylor CR. A comparative autoradiographic study demonstrating differential intratumour localization of monoclonal antibodies to cell surface (Lym-1) and intracellular (TNT-1) antigens. *J Nucl Med* 1990, **31**, 1059–1066.
8. Benke R, Lang E, Komitowski D, Muto S, Schirrmacher V. Changes in tumour cell adhesiveness affecting speed of dissemination and mode of metastatic growth. *Invasion Metastasis* 1988, **8**, 159–176.
9. Matzku S, Kirchgessner H, Schirrmacher V. Antibody targeting to the murine lymphoma ESb-MP: Increased accumulation due to reduced internalization into lymphoma cells as compared to normal lymphoid cells. *Int J Cancer* 1988, **41**, 108–114.
10. Pflüger E, Lang E, Benke R, Heckl-Östreicher B, Altevogt P, Schirrmacher V. Generation of adhesive tumour variants: chromosomal changes, reduction in malignancy and increased expression of a distinct membrane glycoprotein. *Clin Exp Metastasis* 1988, **6**, 485–499.
11. Altevogt P, Michaelis M, Kyewski B. Identical forms of the CD2

antigen expressed by mouse T and B lymphocytes. *Eur J Immunol* 1989, **19**, 1509–1512.
12. Altevogt P, Kohl U, Von Hoegen P, Lang E, Schirrmacher V. Antibody 12-15 cross-reacts with mouse Fc(gamma) receptors and CD2: Study of thymus expression, genetic polymorphism and biosynthesis of the CD2 protein. *Eur J Immunol* 1989, **19**, 341–346.
13. Blasberg RG, Groothuis D, Molnar P. Application of quantitative autoradiographic measurements in experimental brain tumour models. *Semin Neurol* 1981, **1**, 203–221.
14. Davenport AP, Hill R, Hughes J. Quantitative analysis of autoradiograms. *Experimentia* 1989, **56**, 137–153.
15. Hall MD, Davenport AP, Clark CR. Quantitative receptor autoradiography. *Nature* 1986, **324**, 493–494.
16. Schmid U, Bihl H, Matzku S. Antibody accumulation in small tissue samples: Assessment by quantitative autoradiography. *Nucl Med Biol* 1990 (in press).
17. Fraker PJ, Speck JC. Protein and cell membrane iodinations with a sparingly soluble chloroamide, 1,3,4,6-tetrachloro-3α,6α-diphenylglycoluril. *Biochem Biophys Res Commun* 1980, **80**, 849–857.
18. Davenport AP, Hall MD. Comparison between brainpaste and polymer [I^{125}]standards for quantitative receptor autoradiography. *J Neurosc Meth* 1988, **25**, 1–8.
19. Badger CC, Krohn KA, Shulman H, Flournoy N, Bernstein ID. Experimental radioimmunotherapy of murine lymphoma with 131I-labelled anti-T-cell antibodies. *Cancer Res* 1986, **46**, 6223–6228.
20. Simpson JG, Fraser RA. Angiogenese in malignen Tumoren. In Messmer K, Hammersen F, eds. *Progress in Applied Microcirculation*. Basel, Karger, 1983, 1–14.
21. Warren BA. The vascular morphology of tumours. In Peterson H-I, ed. *Tumour Blood Circulation: Angiogenesis, Vascular Morphology and Blood Flow of Experimental and Human Tumours*. Boca Raton, Florida, CRC Press, 1979, 1–47.
22. Cobb LM. Intratumour factors influencing the access of antibody to tumour cells. *Cancer Immunol Immunother* 1989, **28**, 235–240.
23. Sharkey RM, Filion D, Fand I, Primus FJ, Goldenberg DM. A human colon cancer metastasis model for radioimmunodetection. *Cancer Res* 1986, **46**, 3677–3683.
24. Beatty JD, Duda BB, Williams LE, *et al.* Preoperative imaging of colorectal carcinoma with 111In-labelled anticarcino-embryonic antigen monoclonal antibody. *Cancer Res* 1986, **46**, 6494–6502.

Acknowledgements—The expert technical assistance of Marion Stadler, A. Griesbach, and H. Kirchgessner is gratefully acknowledged. G. Sroka and G. Hartmann are thanked for valuable assistance with the computer analysis of digital matrices.

Eur J Cancer, Vol. 29A, No. 2, pp. 225–230, 1993.
Printed in Great Britain

0964–1947/93 $5.00 + 0.00

Suramin-induced Growth Inhibition and Insulin-like Growth Factor-I Binding Blockade in Human Breast Carcinoma Cell Lines: Potentially Related Events

Federica Ravera, Loredana Miglietta, Paolo Pirani, Silvano Ferrini and Roberto E. Favoni

Suramin, a polyanionic drug used in the treatment of trypanosomiasis and onchocerciasis, inhibits growth factor-induced mitogenesis in several human tumours. We have investigated the effect of suramin on human breast cancer cell lines (HBCCL). By cell counts and thymidine incorporation we found that 50 to 400 μg/ml suramin inhibits the proliferation of HBCCL in a dose-dependent and reversible fashion ($ID_{50} \approx 200$ μg/ml for MCF-7 and MDA-MB 231). Radioreceptor and affinity cross-linking assays showed that suramin was also able to reduce the binding of insulin-like growth factor I (IGF-I) to its receptor (40–50% inhibition at 100 μg/ml). Our results indicate that the drug does not affect the IGF-I receptor (IGF-I-R), but binds directly to the IGF-I peptide. In conclusion, the strict correlation observed between suramin inhibition of proliferation and IGF-I binding on HBCCL suggests a possible therapeutic role for this molecule as an antineoplastic drug in human breast tumours.
Eur J Cancer, Vol. 29A, No. 2, pp. 225–230, 1993.

INTRODUCTION

SURAMIN IS a polysulphonated drug that has been used in the treatment of certain parasitic diseases, especially trypanosomiasis and onchocerciasis [1]; it affects cell metabolism in different ways and has been shown to inhibit a large number of enzymatic systems [2]. De Clercq [3] reported that suramin inhibits the reverse transcriptase activity of several avian and murine retroviruses, showing virustatic capacity. Suramin has therefore been tested in clinical trials for the acquired immunodeficiency syndrome [4]; the response noted in an HIV-associated lymphoma indicated the possible use of suramin as an antineoplastic drug [5]. Initial phase I/II studies, which were performed on patients with prostatic [6], adrenal and renal [5, 7] cancer, and also with a variety of lymphomas [5], described partial, minimal as well as no response. Moreover, a correlation between response and serum suramin levels has been shown: most occurred at blood levels above 200 μg/ml but serious toxicity was found for

Correspondence to R. E. Favoni.
F. Ravera, P. Pirani, S. Ferrini and R. E. Favoni are at the Department of Experimental Pharmacology; and L. Miglietta is at the Department of Medical Oncology II, Istituto Nazionale per la Ricerca sul Cancro, Viale Benedetto XV, 10 16132 Genova, Italy.
Revised 19 June 1992; accepted 20 July 1992.